Field Expulsion and Reconfiguration in Polaritonic Photonic Crystals

Kerwyn Casey Huang,* Peter Bienstman, John D. Joannopoulos, and Keith A. Nelson
Center for Materials Science and Engineering, Massachusetts Institute of Technology, Cambridge, Massachusetts 02139, USA

Shanhui Fan
Department of Electrical Engineering, Stanford University, Stanford, California 94305, USA
(Received 23 October 2002; published 13 May 2003)

We uncover a rich set of optical phenomena stemming from the incorporation of polar materials exhibiting transverse phonon polariton excitations into a photonic crystal structure. We identify in the frequency spectrum two regimes in which the dielectric response of the polaritonic medium can induce extreme localization of the electromagnetic energy. Our analysis of the effect of polarization and the interaction between the polariton and photonic band gaps on the Bloch states leads to a pair of mechanisms for sensitive frequency-controlled relocation and/or reconfiguration of the fields.

DOI: 10.1103/PhysRevLett.90.196402 PACS numbers: 71.36.+c, 41.20.–q, 42.70.Qs, 71.15.–m

The incorporation of materials which exhibit transverse phonon polariton excitations in place of frequency-independent dielectrics in photonic crystals produces a novel class of optical structures with remarkable properties that can be tied directly to interplay between the strongly dispersive nature of these polar media and the structural dispersion of the crystal. In this Letter, we demonstrate theoretically that minute variations in certain frequency ranges can induce enormous changes in the fundamental character of the crystal excitations. In particular, we find that the modes can not only exhibit almost complete localization, but the frequency shift is a mechanism by which the electromagnetic energy can be relocated and rearranged in the crystal in a dramatic fashion. These features can occur near the lower boundary of the characteristic polariton photonic band gap in two distinct manners: interband transitions across the boundary induce flux expulsion from the polariton material or the surrounding ambient dielectric, and intraband transitions below the gap produce a polarization-dependent restructuring of the nodes in the field pattern. In addition, our analysis reveals that the existence of both of these phenomena is mediated precisely by the overlap of the polariton gap with the photonic band gaps of a metallodielectric crystal with the same spatial arrangement of metallic rods as of polaritonic rods in the polaritonic photonic crystal (PPC). To illustrate these effects, we provide a complete band structure calculation of a PPC.

A simple yet effective model for the polariton dielectric function is [1],

$$\varepsilon(\omega) = \varepsilon_\infty\left(\frac{\omega^2 - \omega_L^2}{\omega^2 - \omega_T^2}\right), \tag{1}$$

where ε_∞ measures the optical response at high frequency, and ω_L is related to ε_∞ and ω_T through the well-known Lyddane-Sachs-Teller relation $\omega_T\sqrt{\varepsilon(0)/\varepsilon_\infty}$. The choice of photonic crystal and polariton parameters $\{a, \varepsilon_\infty, \omega_T, \omega_L\}$, where a is the lattice constant, is crucially important to the existence of new polariton-associated features. Previous PPC band structure calculations [2–5] have operated in frequency regimes where the main feature is the presence of almost dispersionless bands below ω_T. We present in this work systems in which these flat bands exist in combination with metallic bands above ω_T. Moreover, we demonstrate that the bands below ω_T of TE polarization can in fact have significant bandwidth under certain symmetry conditions. These two properties are intimately related to the position of the polariton gap in relation to the photonic band gaps of the metallodielectric crystal obtained by replacing the polaritonic rods with a perfect metal, and provide the basis for a pair of optical phenomena that we characterize shortly as *flux expulsion* and *node switching*.

In order to study the frequency range around ω_T both efficiently and accurately, we employ a computational technique based on vectorial eigenmode expansion [6]. We divide a unit cell into layers where the index profile does not change in the propagation direction. In each of these layers, we expand the field in the local eigenmodes of that particular layer. The only approximation is the size of the eigenmode basis, which we have determined to be well converged at 40. Using mode matching, we derive frequency-dependent reflection and transmission matrices that completely describe the scattering behavior of the unit cell:

$$\mathbf{F}_2 = \mathbf{T}_{12}\cdot\mathbf{F}_1 + \mathbf{R}_{21}\cdot\mathbf{B}_2, \tag{2}$$

$$\mathbf{B}_1 = \mathbf{R}_{12}\cdot\mathbf{F}_1 + \mathbf{T}_{21}\cdot\mathbf{B}_2. \tag{3}$$

Here, $\mathbf{F}$ and $\mathbf{B}$ are column vectors containing the expansion coefficients of the forward and backward propagating fields, respectively. We then impose Bloch boundary conditions and recast Eq. (2) as a generalized eigenvalue problem, which can be solved for each frequency:

$$\begin{bmatrix} \mathbf{T}_{12} & \mathbf{R}_{21} \\ 0 & \mathbf{I} \end{bmatrix}\begin{bmatrix} \mathbf{F}_1 \\ q\mathbf{B}_1 \end{bmatrix} = q\begin{bmatrix} \mathbf{I} & 0 \\ \mathbf{R}_{12} & \mathbf{T}_{21} \end{bmatrix}\begin{bmatrix} \mathbf{F}_1 \\ q\mathbf{B}_1 \end{bmatrix},$$

where $\mathbf{I}$ is the unit matrix and $q = e^{-ika}$. Since the independent variable in these calculations is frequency, it is trivial to account for any frequency-dependent dielectric response, unlike time-domain or plane-wave methods. These techniques were implemented in our generic photonic simulation tool CAMFR, which is freely available from http://camfr.sourceforge.net.

In Fig. 1, we plot the band structure from Γ to X of a 2D photonic crystal of square rods with side s ($s/a = 0.25$) in a square lattice. The rods are taken to be $LiTaO_3$, a typical polaritonic material with a large polariton gap from $\omega_T = 26.7$ THz to $\omega_L = 46.9$ THz, and $\varepsilon_\infty = 13.4$. We set $a = 29.7$ μm so that $\omega_T = 0.4(2\pi c/a)$ and $\omega_L = 0.703(2\pi c/a)$. We overlay with dashed lines the band structure for the metallodielectric crystal obtained by replacing $LiTaO_3$ with a perfect metal. In addition, we highlight the most important sections: directly above and below ω_T. The frequency range $[\omega_T, \omega_L] = [0.4, 0.703] \times (2\pi c/a)$ is labeled the *polariton gap*.

Note the existence of flat bands in both polarizations in the high-index region below ω_T, as observed in earlier work [2,3]. We find that these bands correspond extremely closely to localized resonance modes [7] in isolated rods with slight dispersion about a frequency (to within less than 1% error in most cases) given by the following analytic expression:

$$\hat{\omega}_{lm}^2 = \tfrac{1}{2}[\omega_L^2 + \Omega_{lm}^2 - \sqrt{(\omega_L^2 + \Omega_{lm}^2)^2 - 4\Omega_{lm}^2\omega_T^2}], \quad (4)$$

where $\Omega_{lm} = \pi c(l^2 + m^2)^{1/2}/s\sqrt{\varepsilon_\infty}$. However, there are many other TE bands with a much larger bandwidth that are roughly linear, except near the resonance frequencies $\hat{\omega}_{lm}$, where they rapidly flatten. Away from these resonances, the TE bands show a remarkable tendency to mimic the lowest band of the metallodielectric crystal previously introduced.

The differences between TE and TM modes are derived from the relative locations of the photonic band gaps of the metallodielectric crystal to the polariton gap. When the index of refraction n is much greater than one, the reflectivity $R = |(n-1)/(n+1)|^2 \to 1$ on both sides of the polariton-vacuum interface. The states with flux situated in the ambient space are precisely the bands of the metallodielectric crystal, and it is these bands (if they exist) to which the highly localized resonance modes $\hat{\omega}_{lm}$ of the polaritonic rods can couple

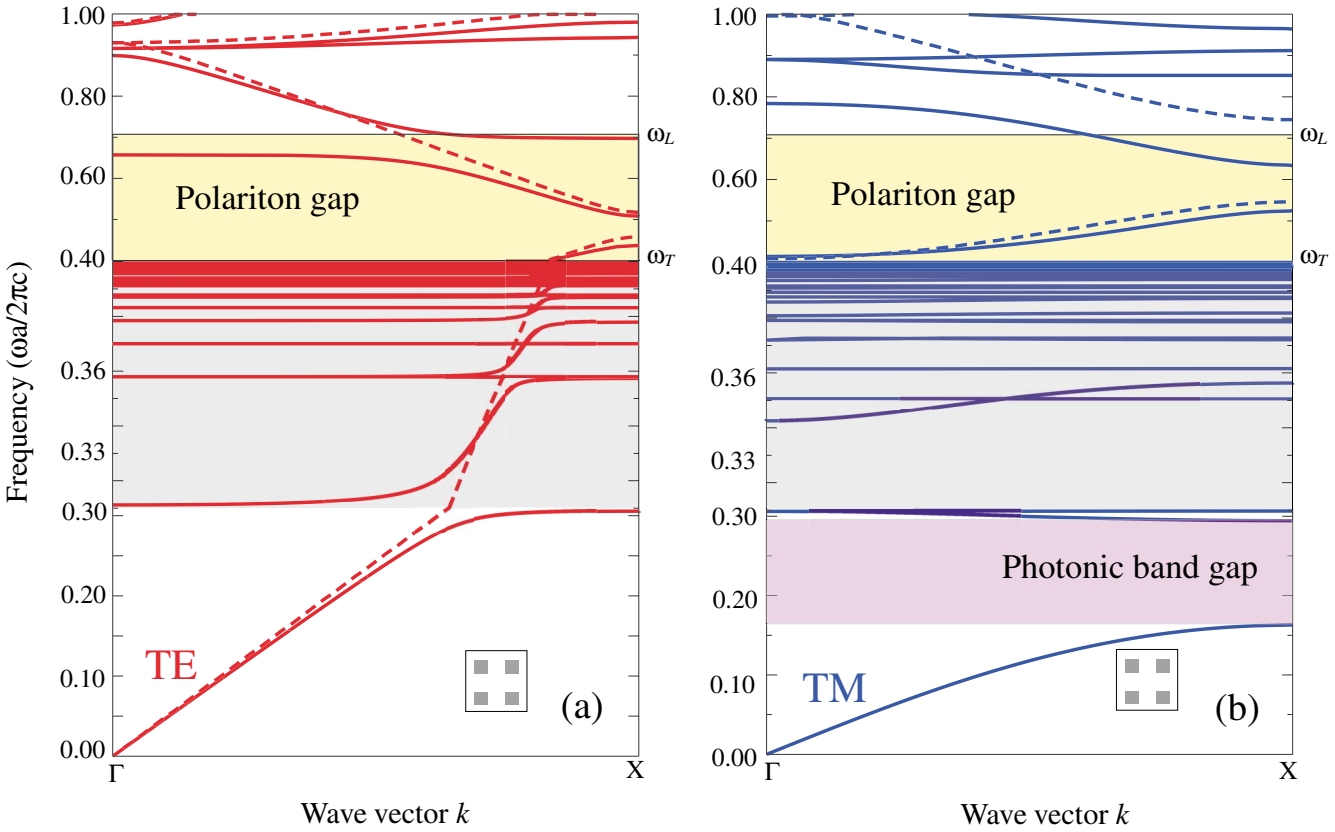

FIG. 1 (color). Band structure of a 2D polaritonic photonic crystal with square symmetry of square $LiTaO_3$ rods in air with $s/a = 0.25$, $\omega_T = 0.4(2\pi c/a)$, $\omega_L = 0.703(2\pi c/a)$, and $\varepsilon_\infty = 13.4$. The TE ($\mathbf{H}$ out of plane) bands are in red in (a), TM ($\mathbf{E}$ out of plane) in blue in (b). Note the three different frequency spacings for the intervals $[0, 0.31](2\pi c/a)$, $[0.31, 0.4](2\pi c/a)$ (shaded in gray), and $[0.4, 1.0](2\pi c/a)$. The primary photonic band gap in the TM modes is indicated by purple shading. The TE (TM) bands of a metallodielectric crystal obtained by replacing $LiTaO_3$ by a perfect metal are given by the red (blue) dashed lines.

in an anticrossing interaction. This produces the high dispersion TE bands below ω_T which are present in Fig. 1. Since the metallodielectric crystal has a TM band gap from zero frequency to $0.409(2\pi c/a)$, this coupling is possible only for the TE modes below ω_T when $\omega_T = 0.4(2\pi c/a)$.

However, no anticrossing of this nature can occur involving any of the modes near the frequencies $\hat{\omega}_{2l,2m}$, resulting in, e.g., the flat band near $\hat{\omega}_{22} = 0.373(2\pi c/a)$. This is due entirely to symmetry: the real part of H_z has a node on both Cartesian axes going through the center of the rod. Because of this, there is no interaction with the lowest metallodielectric state, which has a magnetic field with even symmetry upon reflection about one of the axes. For the same reason, one out of the two degenerate $(2l+1, 2m)$ states will be noninteracting; hence, there is a flat band near $\hat{\omega}_{12} = 0.359(2\pi c/a)$ at the edge of the band joining $\hat{\omega}_{21}$ and $\hat{\omega}_{31}$.

This anticrossing interaction has important implications for the field orientations of the Bloch states with $\omega < \omega_T$. The magnetic field of the TE states near the band edges bears a close resemblance to the highly localized resonance mode of the polaritonic rod to which it is closest in frequency. Consider one of the several resonance pairs (l, m), (l', m') with a very small frequency separation that are connected by a TE band through this interaction, such as $\hat{\omega}_{33} - \hat{\omega}_{41} = 0.0007(2\pi c/a)$. Along this band, the nodal structure of the field inside the rod, perpendicular to the plane, is forced to continuously mutate from one pattern to another, as shown in Fig. 2. This node switching phenomenon provides an unprecedented capability to drastically alter the coupling behavior of a localized state over a very small frequency range.

The crystal excitations in the frequency domain $\omega > \omega_T$ are strikingly unlike the rod-localized states below ω_T. As ω approaches ω_T from above, ε becomes extremely negative, and so the polaritonic material behaves as a metal. Hence, when ω_T overlaps with one of the metallodielectric crystal bands, a PPC band of the same polarization exists inside the polariton gap which converges to the metallodielectric band as $\omega \to \omega_T$. In our calculation with $\omega_T = 0.4(2\pi c/a)$, ω_T is outside the TE metallodielectric band gap from $[0.458, 0.517] \times (2\pi c/a)$ and inside the TM band gap $[0, 0.409](2\pi c/a)$. Correspondingly, we see in Fig. 1 that there is a TE PPC band that intersects ω_T, at $k = 0.432\pi/a$, but no TM PPC band directly above ω_T; the lowest frequency TM-polarized state above ω_T is at $k = \Gamma$, $\omega = 0.415(2\pi c/a)$.

It is clear from our discussion of how flux can be isolated to either of the two opposite physical regions of the crystal that small changes in ω can induce enormous variations in the field profiles due to the rapid change in ε. In Fig. 3(a), we explore an interband transition at fixed wave vector from below ω_T to a frequency inside the polariton gap. The light is transferred almost completely from inside the rod at $\omega = 0.3916(2\pi c/a)$ [Fig. 3(b)] to

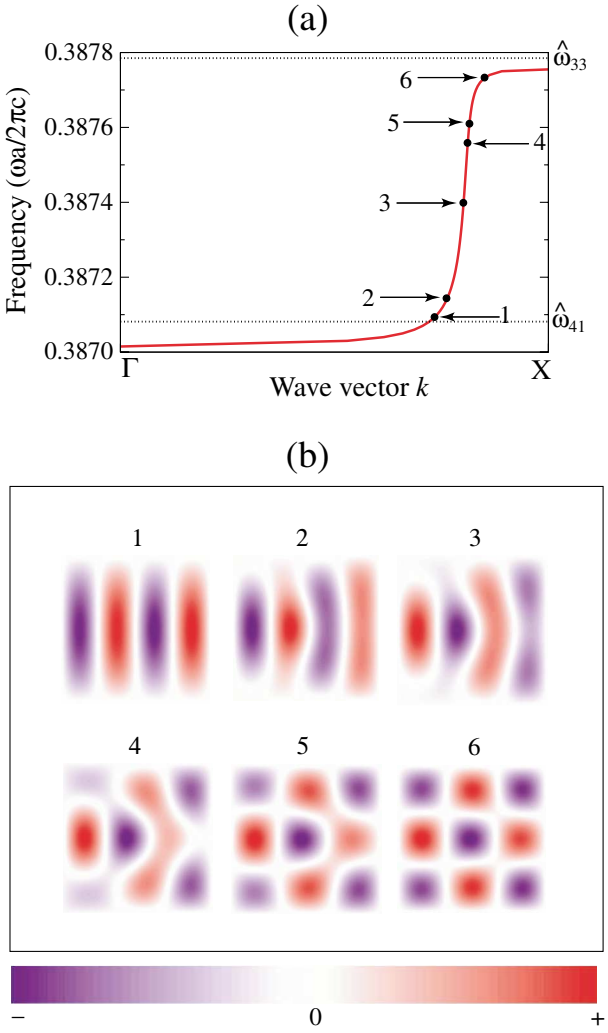

FIG. 2 (color). Node switching: (a) the TE band connecting the (4,1) cavity mode to the (3,3) cavity mode of a 2D PPC with square rods of $LiTaO_3$, $s/a = 0.25$, with selected frequencies indicated by the numbered arrows. (b) The real part of H_z inside the rods at the frequencies indicated in (a) between $0.3871(2\pi c/a)$ and $0.38775(2\pi c/a)$.

the ambient region at $\omega = 0.403(2\pi c/a)$ [Fig. 3(c)]. With a wide range of options in terms of crystal geometries and ambient materials, the utility of this flux expulsion is manifest. For example, using a nonlinear material as the surrounding medium, this phenomenon could be utilized as a switch to shift light in and out of different physical regions of the crystal.

In order to incorporate losses in the polaritonic material, a more accurate model for the dielectric function is

$$\epsilon(\omega) = \varepsilon_\infty\left(1 + \frac{\omega_L^2 - \omega_T^2}{\omega_T^2 - \omega^2 - i\omega\Gamma}\right), \tag{5}$$

where Γ represents the width of the absorption peak in $\mathrm{Im}[\varepsilon(\omega)]$. Sigalas *et al.* implemented Eq. (5) in transmission calculations to determine the photonic band gaps

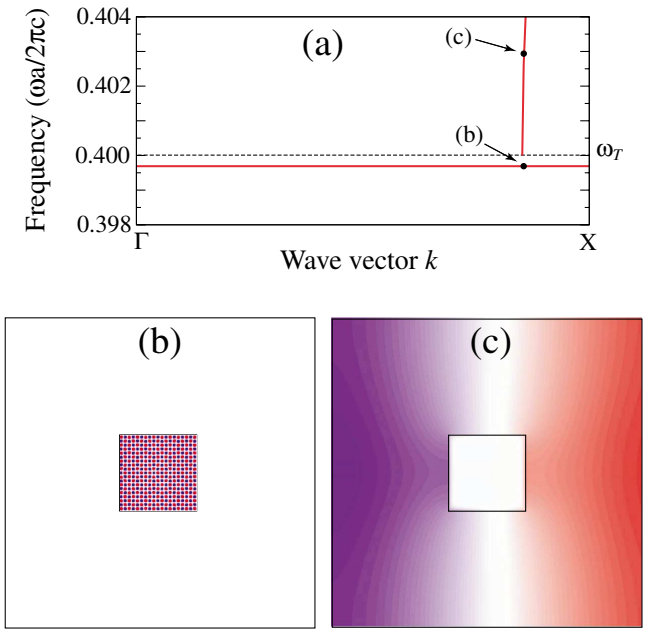

FIG. 3 (color). Flux expulsion: (a) the band directly above ω_T and a flat band just below ω_T in a 2D PPC of $LiTaO_3$ rods with $s/a = 0.25$ with the frequencies $\omega = 0.3916(2\pi c/a)$ and $\omega = 0.403(2\pi c/a)$ marked by black dots. The wave vector at both of these frequencies is $0.43(2\pi/a)$. (b) The field pattern of the real part of H_z at $\omega = 0.3916(2\pi c/a)$, where $\varepsilon = 649$. (c) The field pattern of the real part of H_z at $\omega = 0.403(2\pi c/a)$, where $\varepsilon = -1773$. Note the extreme contrast between the localization of the field inside the rod in (b) and the complete flux expulsion in (c).

in a PPC [8]. Along the ordinary axis of the $LiTaO_3$ crystal, $\Gamma = 0.94$ THz $= 0.013(2\pi c/a)$. Although we have focused in this Letter on instances of optical phenomena very close to ω_T, these effects will also occur well away from ω_T. The second TE band in the PPC exhibits a transition from the $\hat{\omega}_{11}$ to the $\hat{\omega}_{21}$ localized rod state, ending at the frequency $0.36(2\pi c/a)$. Moreover, the TE band ending at ω_T inside the polariton gap extends to above $0.44(2\pi c/a)$. Therefore, the node switching and flux expulsion phenomena can be realized with states removed from ω_T by at least 3Γ. Hence, the perturbations to these states due to losses are negligible, allowing for their experimental observation in a physical crystal. Key to this argument are the large value of $\varepsilon_0 = 41.4$ and the small ratio $\Gamma/\omega_T = 0.032$. Indeed, we have verified these conclusions by explicity including losses in select calculations for this PPC system.

Our research has provided compelling support for inclusion of the vectorial eigenmode expansion method in the toolkit of techniques such as the layer-Korringa-Kohn-Rostoker method [9] and the multiple multipole method [10], applicable not only for PPCs but any system of materials with a frequency-dependent optical response. For our needs, it provides the means to tackle more complicated problems involving polaritonic photonic crystals, including dissipative systems and more complicated crystal structures. We have as yet not studied either the band structure between Γ and K or nonsquare geometries due to the increased computation that would be necessary using this technique, but we believe that all of our ideas should apply conceptually without any major modifications.

In conclusion, we have discovered two novel optical phenomena resulting from the localization capabilities of the polaritonic material in the adjacent frequency regimes above and below ω_T. A complete change in the symmetry of the field pattern can be effected across a single band in the high-index regime, and light can be completely relocated into and out of the polariton material by varying the frequency across the ε discontinuity. The ability to vary the size of the rods and the translational symmetry group of the crystal should provide an additional measure of tuneability to make it easier to isolate the effects described in this work.

K. C. H. thanks Michelle Povinelli, Elefterios Lidorikis, and Steven Johnson for many useful discussions. Funding was provided the MRSEC program of the NSF under Grant No. DMR-0213282. P. B. acknowledges support from the Flemish Fund for Scientific Research (FWO-Vlaanderen).

*Electronic address: kch23@mit.edu

[1] C. Kittel, *Introduction to Solid State Physics* (John Wiley & Sons, Inc., New York, NY, 1966), 7th ed.
[2] W. Zhang, A. Hu, X. Lei, N. Xu, and N. Ming, Phys. Rev. B **54**, 10 280 (1996).
[3] V. Kuzmiak, A. A. Maradudin, and A. R. McGurn, Phys. Rev. B **55**, 4298 (1997).
[4] A. Y. Sivachenko, M. E. Raikh, and Z. V. Vardeny, Phys. Rev. A **64**, 013809 (2001).
[5] N. Eradat, A. Y. Sivachenko, M. E. Raikh, and Z. V. Vardeny, Appl. Phys. Lett. **80**, 3491 (2002).
[6] P. Bienstman and R. Baets, Opt. Quantum Electron. **33**, 327 (2001).
[7] E. Lidorikis, M. M. Sigalas, E. N. Economou, and C. M. Soukoulis, Phys. Rev. Lett. **81**, 1405 (1998).
[8] M. M. Sigalas, C. M. Soukoulis, C. T. Chan, and K. M. Ho, Phys. Rev. B **49**, 11 080 (1994).
[9] A. Modinos, N. Stefanou, and V. Yannopapas, Opt. Express **8**, 197 (2001).
[10] E. Moreno, D. Erni, and C. Hafner, Phys. Rev. B **65**, 155120 (2002).